Measurement of Specific Absorption Rate and Thermal Simulation for Arterial Embolization Hyperthermia in the Maghemite-Gelled Model

Ruizhi Xu, Yu Zhang, Ming Ma, Jingguang Xia, Jiwei Liu, Quanzhong Guo, and Ning Gu

Department of Biological Science and Medical Engineering, Jiangsu Laboratory for Biomaterials and Devices, State Key Laboratory of BioElectronics, Southeast University, Nanjing 210096, China

Theoretical models are designed to be applied in hyperthermia treatment planning and to help optimize the surgical treatment procedures. However, it is difficult to obtain every physical parameter of the magnetic field in the living tissue in detail, which is necessary for the calculation. We therefore investigated the simulation of thermal distribution in arterial embolization hyperthermia (AEH) stimulated by the external ferrite-core applicator, and measured specific absorption rate (SAR) of magnetic nanoparticles in the maghemtite-gelled composite model. We used fiber optic temperature sensors (FOTS) to measure the values of SAR, which depend on the microstructure and sizes of particles and the intensity and frequency of external ac magnetic field. Detailed tests indicated that the attenuation of magnetic field was mainly focused on the vertical distance in the aperture of the apparatus. We built a simplified cylindrical phantom containing maghemite particles of 20 nm for thermal field simulation on the basis of SAR measurement. The results of simulation indicated that temperature elevation, induced by nanoparticles inside tumors under ac magnetic field, was dose-dependent. The temperature data acquired from the experiment were compatible with the theoretical results, which demonstrated that the current model considering the inhomogenous heat generation could provide accurate and reliable simulation results and a theoretical and technical basis for controlling temperature during AEH therapy.

Index Terms—**Arterial embolization hyperthermia, maghemite particles, mathematical modeling, specific power absorption.**

I. Introduction

MAGNETIC fluid hyperthermia (MFH) [1], [2] selectively heats up tumors to temperatures of 42 °C–45 °C [3] by forcing ac magnetic fields on biocompatible magnetic iron oxide nanoparticles (NPs) such as Fe_3O_4 γ-Fe_2O_3, which exhibit an extraordinary specific absorption rate (SAR[W/g]) on the basis of the Néel relaxation and Brownian rotation losses [4]. In recent years, many investigations were carried out, especially some experiments *in vivo* on animals with prostate cancer [5], renal tissue [6], and liver tumors [7], etc., to make preparation for applying to human patients. In contrast with the heat generated by external electrodes, microwaves or ultrasound, MFH can heat deep-situated tumors instead of overheating the superficial healthy tissues; while compared with implanted electrodes, invasive microwave antennas, and thermal seed heating, MFH can alleviate invasive pain maximally [8].

Arterial embolization hyperthermia (AEH) is one of the therapeutic methods of MFH [6]. The lipiodol, in which magnetic nanoparticles are homogenously dispersed, is injected super-selectively through the micro-catheter into the arteries which provide nourishment for tumor cells. When embolization occurs, the tumor tissues containing the magnetic nanoparticles can be heated up by the ac magnetic field at clinically tolerable $H_0 f$ combinations [1].

Diagnosis and treatment relative to hepatocellular carcinoma (HCC) are challenging problems in the world. Surgical resection, hepatic arterial chemotherapy (HAC), selective internal radiation therapy (SIRT), transcatheter arterial chemotherapy embolization (TACE), and ultrasound (US)-guided percutaneous ethanol injection therapy (PEIT), etc., are the present treatments for HCC. Although these treatments have at times shown promising response rates and symptom palliation and have occasionally downstaged hepatic tumors to allow surgical resection, they have not improved five-year survival rates, which remain on the order of less than 1% [7], [9]. AEH is based on selective arterial embolization of liver tumors through lipiodol containing magnetic particles. On one hand, it can cut off the blood supply from the hepatic arterial system to tumors; on the other hand, with the external ac magnetic field it can heat up local tumor tissue through hyperthermia. This new method could be applied to clinical therapy and will have a promising future.

Tumor hyperthermia requires accurate calculation and description of the temperature distribution induced by ac magnetic field in the tissue before it is applied in clinical trial. The temperature distribution inside as well as outside the target region must be known as function of the exposure time in order to provide safe range of therapeutic temperature and, so as to avoid overheat and damage to the surrounding normal tissue [10].

The thermal models are established to simulate the temperature distribution in the tissue, which would be applied in the hyperthermia treatment planning and to help optimize the surgical treatment procedures. In the models [10]–[13], the heat

Digital Object Identifier 10.1109/TMAG.2006.888737

Color versions of one or more of the figures in this paper are available online at http://ieeexplore.ieee.org.

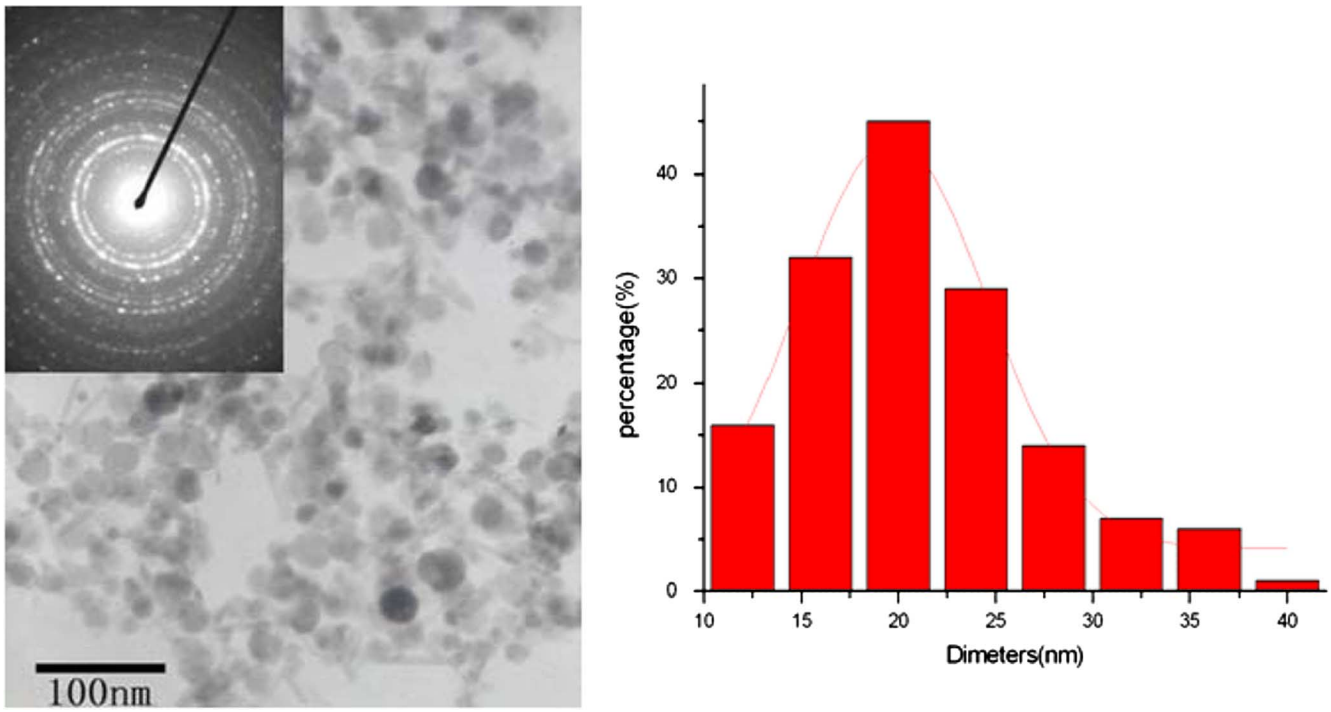

Fig. 1. TEM micrographs of maghemite particles with 20 nm diameters, which were homogeneously distributed in the cylindrical composite, induced by the ac magnetic field and acting as thousands of little heat sources.

generation by the magnetic particles is considered as a constant in the heat transfer equation. Actually, the heat generation rate should be considered as a function of the coordinates, the electrical and magnetic properties of the tissue, and the parameters of the external high-frequency generator [8], [12]. The heterogeneous heat generations in the tissue will lead to inappropriate heating and unexpected temperature scales, although it is difficult to obtain every physical parameter of magnetic field in the living tissue in detail by experiment.

The purpose of our investigation was to establish a model which can realize the detection of inhomogeneous heat generations induced by the external magnetic field, then provide the feasibility of calculation of temperature distribution in the tumor tissue. SAR was determined by the initial temperature transient in the maghemite-gelled composite. The different values of the relative different locations along the perpendicular axis implied the magnetic field attenuation of the apparatus. Moreover, the SAR distribution was used in conjunction with a cylindrical model to determine the temperature field. The progressional solution strategy was implemented to solve the transient heat transfer problem and the results of the simulation reliability were also examined through comparison with experimental data.

II. Material and Theoretical Model

A. Material and Equipment

The material used in the experiment involved the following steps. First, the nanoparticles with diameters of 20 nm (see Fig. 1) were mixed with the gelose solution. Second, the mixture was heated to its melting point. Third, the gel suspension was cooled down. Finally, the cylindrical composite formed (see Fig. 2).

Fig. 2. Temperature Elevation Experiment: The cylindrical maghemite-gelled composite was located in the device aperture. Six optic fibers were inserted into the composite to measure the temperature. When the device power was switched on, the ac magnetic field was produced and the cylindrical composite was heated up.

The AEH therapy system has been set up at Jiangsu Laboratory for Biomaterials and Devices. The system mainly consists of a ferrite-core applicator with the aperture (vertical distance: 350 mm, length 300 mm, and width 200 mm). The device is operated at a frequency of 80 kHz. The field strength can be adjusted from 0 to 10 kA/m (see Fig. 3).

The eight-channel fiber-optic thermometry device (FISO Technologies Corp., CA, accuracy: $\pm 0.3^{\circ}$) was introduced in

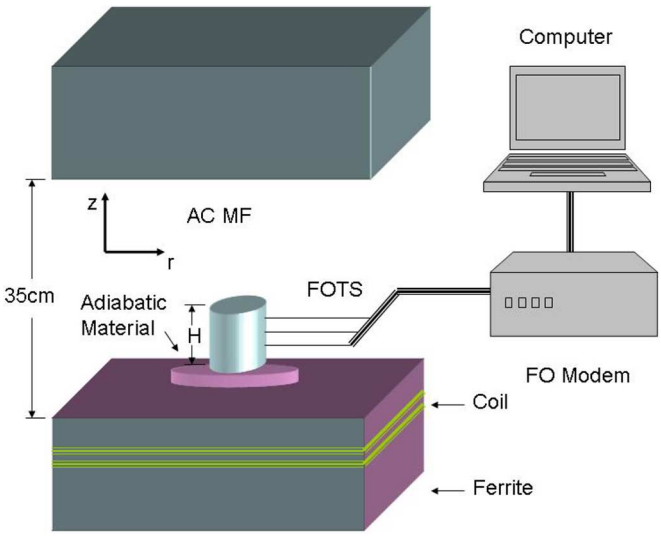

Fig. 3. Scheme of the ferrite-core-applicator operating system.

the Temperature Elevation Experiment (see Fig. 2), involving six fibers inside a cylindrical composite which can be used to detect temperature changes and two others for monitoring the ascending temperature of the ferrite core to avoid unsafe work.

B. Study of SAR in Pennes' Equation

The thermal models have been established such as the earliest Pennes (BHT) Model [14], the Chen and Holmes (CH) Model [15], and the Weinbaum-Jiji and Lemons (WJL) Model [16], etc. The Pennes model for describing heat transfer in a tissue, originally designed for predicting temperature fields in the human forearm, has become well known as the "bio-heat transfer" equation [14]. The CH model of bio-heat transfer is obtained by replacing the single perfusion term in the Pennes model with the vascular contributions [15]. The WJL model is based on completely different vascular generations: the WJL equations apply to thermally significant small vessels and not to major supply blood vessels [16].

Due to its conciseness and validity, up to now, nearly all the property measurements are based on the well-known Pennes' bio-heat equation, which is written as [14]

$$\rho C\frac{\partial T}{\partial \tau} = \nabla\cdot(K\nabla T) + \omega_b C_b(T_a - T) + Q_m + Q_r \quad (1)$$

where ρ is density of the tissue (kg/m^3), C is specific heat of tissue (J/kg°C), T is tissue temperature, τ is time (s), K is thermal conductivity of tissue (W/m°C), ω_b is blood perfusion rate (kg/m^3), C_b is specific heat of blood (J/kg°C), Q_m is the thermoregulation mechanisms of the biological bodies, and Q_r is heat generation due to external heat source, respectively (W/m^3).

The research shows that little eddy-current heating occurred in the deeply situated tissue, while a greater amount of heating was produced in the more superficial tissues when the animal was exposed to the magnetic field with 0.034 T and 20 kHz [6]. In our study, eddy currents induced in the gel without NPs under the device condition (10 kA/m and 80 kHz) results in only a slight additional tissue heating. Therefore, the most likely contributing factor to local temperature elevation is the heat generation of magnetic nanoparticles.

For small field amplitudes, and assuming minimal interactions between the constituent magnetic particles, the response of the magnetization of a ferrofluid to an ac field can be described in terms of its complex susceptibility

$$\chi = \chi' + i\chi'' \quad (2)$$

where both χ' and χ'' are frequency dependent.

$$P = \mu_0\pi f\chi''|H|^2 \quad (3)$$

is given by [17] and [18], where P is heat generation of nanoparticles, H the amplitude of the magnetic field intensity, and $\mu_0 = 4\pi\times 10^{-7}$ T·m·A^{-1}.

However, the physical parameters of magnetic field inside the tissues could not be directly measured, when the above formulas are provided for theoretical calculation.

The temperature distribution may be directly related to the SAR distribution [3]. The heat generation of magnetic particles is given as [10]

$$Q_r = \mathrm{SAR}\cdot m/V \quad (4)$$

where m means the iron-oxide mass and V is the volume of the composite.

Actually in the clinical therapy, the magnetic particle spatial distribution is not homogeneous in the whole bulk of tissue region. It can be identified by computed tomography (CT). Define ξ_{Fe} or ξ_{NP} as the bulk of tissue unit containing the mass of the element Fe of or the nanoparticles (NPs) (g of Fe/m^3 or g of NP/m^3)

$$\iiint_{\Omega tiss}\xi_{\mathrm{Fe}}(x,y,z)dV = m_{\mathrm{Fe}} \quad (5a)$$

$$\iiint_{\Omega tiss}\xi_{\mathrm{NP}}(x,y,z)dV = m_{\mathrm{NP}} \quad (5b)$$

where m_{Fe} is the total mass of element Fe and m_{NP} the nanoparticles in the tissue.

SAR is a function of H_i and f [10]. In fact, the value of H_i is a function of space as a consequence of the attenuation of the magnetic field. Then we can conclude that

$$Q_r = \mathrm{SAR}(x,y,z)\cdot\xi_{\mathrm{Fe}}(x,y,z). \quad (6)$$

C. Measurement of SAR

According to (4)

$$\mathrm{SAR} = C\frac{\Delta T}{\Delta\tau}\frac{1}{m_{\mathrm{Fe}}} \quad (7)$$

where C is the sample-specific heat capacity which is calculated as a mass weighted mean value of magnetite and water. $\Delta T/\Delta\tau$

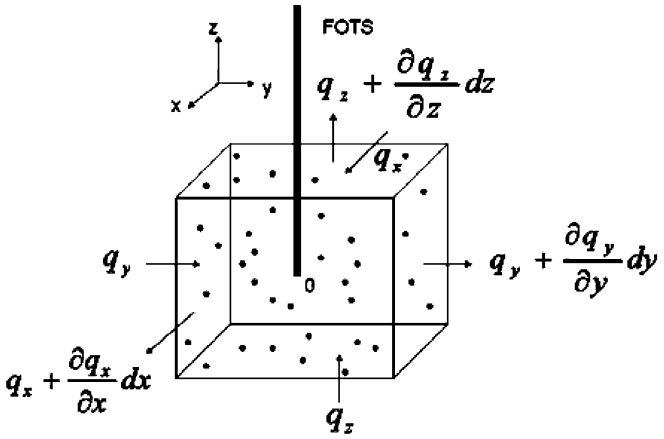

Fig. 4. Scheme of a small unit of tissue containing the magnetic nanoparticles, where q is the density of heat generation. The optic fiber is used for measuring the value of SAR at the central spot *in vitro*. The slope of temperature ascending curve at the initial time means the value of $Q_r/\rho C$.

is the initial slope of time-dependent temperature curve. m_{Fe} is the iron content per gram of the Fe_3O_4 or γ–Fe_2O_3 suspension solution. Here the physical parameters (H_0 and f) of ac magnetic field are taken as constants, although the actual field intensity is inhomogeneous in the aperture.

SAR Measurement in Vitro Phantom: The blood perfusion ω_b and the thermoregulation mechanisms Q_m are neglected *in vitro* model. The heat transfer equation is

$$\rho C\frac{\partial T}{\partial \tau} = K\left(\frac{\partial^2 T}{\partial x^2} + \frac{\partial^2 T}{\partial y^2} + \frac{\partial^2 T}{\partial z^2}\right) + Q_r \tag{8}$$

where $Q_r = \mathrm{SAR}(x,y,z)\cdot\xi_{\mathrm{Fe}}(x,y,z)$.

At the instant, the device power is switched on, the conduction heat transfer in the phantom is negligible, and the partial derivative of temperature is in respect to the SAR [9]

$$\left.\frac{\partial^2 T}{\partial x^2} + \frac{\partial^2 T}{\partial y^2} + \frac{\partial^2 T}{\partial z^2}\right|_{\tau=0} = 0 \tag{9a}$$

$$\left.\rho\, C\frac{\partial T}{\partial \tau}\right|_{\tau=0} = \mathrm{SAR}(x,y,z)\cdot\xi_{\mathrm{Fe}}(x,y,z). \tag{9b}$$

When in a small unit of the composite (see Fig. 4), the distribution of nanoparticles can be taken as homogenization

$$\xi_{\mathrm{Fe}}(x,y,z) = \xi_i \tag{10a}$$

where ξ_i is a constant; therefore, the value of SAR at a spatial spot is

$$\mathrm{SAR}(x,y,z) = \rho\, C\left.\frac{\partial T}{\partial \tau}\right|_{\tau=0}/\xi_i \tag{10b}$$

D. The Two-Dimensional Model and Formulation

With different principles, several attempts to simulate hyperthermia have been published in the past. The accuracies of corresponding numerical simulations were, however, hindered mainly by uncertainties of the factors *in vivo*: the effect of blood perfusion and the heat generation by thermoregulation mechanisms.

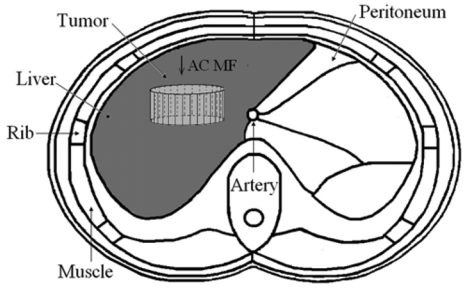

Fig. 5. Scheme of arterial embolization hyperthermia applied to a hepatocellular carcinoma. The small tumor region contains injected magnetic nanoparticles.

It is well known that the blood supply between hepatic tumors and normal liver is different. The macroscopic liver tumors derive virtually all their blood supply from the hepatic arterial system, while normal liver tissue receives most of its blood supply from the portal venous system. This difference in blood supply has been successfully exploited in treatment modalities such as HAC, SIRT, and TACE, which have targeted liver tumors with chemotherapeutic agents and radiation [7]. In our model, when embolization occurs in the artery, there will be much lower blood perfusion in the tumor tissue than normal, reducing the cooling effect.

Therefore, we restrict the following considerations to a simplified model. In this case, the perfusion and heat generation by thermoregulation mechanisms may not be taken into account in the heat conduction equation. Our objective, with the measurement of SAR, is to compare the simulation with the results from experiments *in vitro*.

Let us assume (see Fig. 5) the heat generation Q_r by magnetic particles is concentrated within a small cylinder of radius R and height H with homogeneous heat conductivity K. The heating material, e.g., magnetic particles, which are uniformly dispersed into the cylindrical medium, and the surrounding medium are characterized by the values of their heat convection h, their specific heat capacity C, and their mass density ρ. Because of the cylindrical symmetry of the system, the temperature distribution depends on distance r from the center, vertical distance z from the bottom and on time τ. Thus, our problem is ruled by the differential equation of heat conduction

$$\rho C\frac{\partial T}{\partial \tau} = K\left(\frac{\partial^2 T}{\partial r^2} + \frac{\partial^2 T}{\partial z^2}\right) + Q_r. \tag{11}$$

The initial condition

$$\Delta T(\tau,r,z) = 0 \text{ when } \tau = 0 \tag{12a}$$

$$\Delta T(\tau,r,z) \to \Delta T(r,z) \text{ when } \tau \to \infty \text{ (steady state)} \tag{12b}$$

$$\left.\frac{\partial T(\tau,r,z)}{\partial r}\right|_{r=0} = 0 \quad \text{and} \quad \left.\frac{\partial T(\tau,r,z)}{\partial z}\right|_{z=0} = 0 \tag{12c}$$

the boundary conditions

$$K \cdot \left.\frac{\partial T(\tau,r,z)}{\partial r}\right|_{r=R} + h \cdot \Delta T(\tau,r,z)|_{r=R} = 0,$$

and

$$K \cdot \left.\frac{\partial T(\tau,r,z)}{\partial r}\right|_{z=H} + h \cdot \Delta T(\tau,r,z)|_{z=H} = 0. \quad (12d)$$

Progressional Solution Strategy: From the experiments, the attenuation of the intensity of magnetic field inside depends mainly on the vertical distance z from bottom, while r dependent attenuation is so slight that we can take Q_r only as the distance z dependent power density. From the values of heat generation at some spots measured, the function $Q_r(z)$ can be concluded by a curve fitting technique.

Then we can construct a progressional formulation to $\Delta T(\tau,r,z)$

$$\begin{aligned}\Delta T(\tau,r) &= T(\tau,r,z) - T(\tau,r,z)|_{\tau=0} \\ &= A \cdot \sum_{n=1}^{\infty} \left[1 - \exp\left(-a\beta_n^2\tau\right)\exp\left(-a\gamma_n^2\tau\right)\right] \cdot \cos(\beta_n r) \cdot \cos(\gamma_n z) \\ &+ B \cdot \sum_{n=1}^{\infty} \left[1 - \exp\left(-a\beta_n^2\tau\right)\exp\left(-a\gamma_n^2\tau\right)\right] \cdot \sin(\beta_n r) \cdot \sin(\gamma_n z)\end{aligned} \quad (13)$$

where thermal diffusibility $a = \frac{K}{\rho C}$, A, B, β_n, and γ_n are the coefficients to be determined.

According to (12c), then $B = 0$; to (12d), then

$$tg(\beta_n R) = \frac{h}{\beta_n K} = \frac{hR/K}{\beta_n R} = \frac{B_i}{\beta_n R} \quad (14a)$$

$$tg(\gamma_n H) = \frac{h}{\gamma_n K} = \frac{hH/K}{\gamma_n H} = \frac{B_i}{\gamma_n H} \quad (14b)$$

where B_i is the Biot number, β_n and γ_n can be solved by (14a) and (14b)

$$\begin{aligned}\frac{\partial T}{\partial \tau} &= A \cdot \sum_{n=1}^{\infty} a\left(\beta_n^2 + \gamma_n^2\right) \\ &\cdot \exp\left(-a\beta_n^2\tau\right) \cdot \exp\left(-a\gamma_n^2\tau\right) \cdot \cos(\beta_n r) \cdot \cos(\gamma_n z)\end{aligned} \quad (15a)$$

$$\begin{aligned}\frac{\partial^2 T}{\partial r^2} &= A \cdot \sum_{n=1}^{\infty} \left(-\beta_n^2\right)\left[1 - \exp\left(-a\beta_n^2\tau\right)\right. \\ &\left.\cdot \exp\left(-a\gamma_n^2\tau\right)\right] \cdot \cos(\beta_n r) \cdot \cos(\gamma_n z)\end{aligned} \quad (15b)$$

$$\begin{aligned}\frac{\partial^2 T}{\partial z^2} &= A \cdot \sum_{n=1}^{\infty} \left(-\gamma_n^2\right)\left[1 - \exp\left(-a\beta_n^2\tau\right)\right. \\ &\left.\cdot \exp\left(-a\gamma_n^2\tau\right)\right] \cdot \cos(\beta_n r) \cdot \cos(\gamma_n z).\end{aligned} \quad (15c)$$

By the differential equation (11), then

$$A \cdot \sum_{n=1}^{\infty} \left(\beta_n^2 + \gamma_n^2\right) \cos(\beta_n r) \cos(\gamma_n z) = \frac{Q_r(z)}{K} \quad (16a)$$

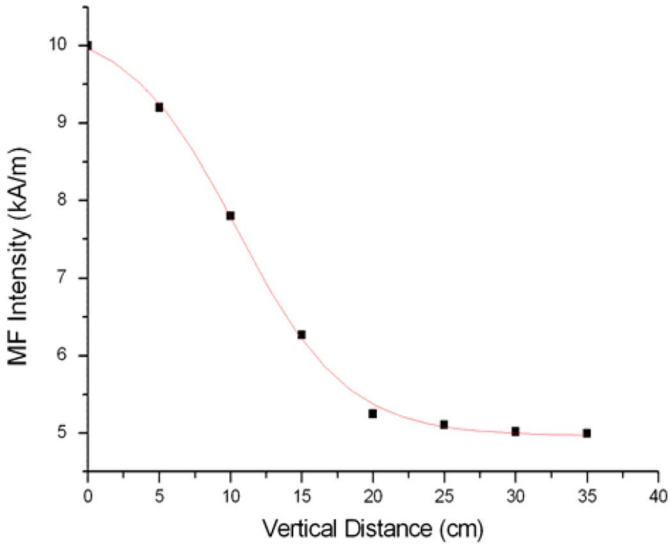

Fig. 6. Attenuation of ac magnetic field intensity with the vertical distance from the bottom of the aperture.

$$\begin{aligned}&A \cdot \sum_{n=1}^{\infty} \left(\beta_n^2 + \gamma_n^2\right) \cdot \int_0^R \cos(\beta_n r)dr \cdot \int_0^H \cos(\gamma_n z)dz \\ &= \frac{1}{K}\int_0^R dr \int_0^H Q_r(z)dz\end{aligned} \quad (16b)$$

$$A = \frac{R}{K} \cdot \frac{\int_0^H Q_r(z)dz}{\sum_{n=1}^{\infty} \frac{\beta_n^2+\gamma_n^2}{\beta_n\gamma_n} \cdot \sin(\beta_n R)\sin(\gamma_n H)}. \quad (17)$$

Then

$$\begin{aligned}\Delta T(\tau,r,z) &= \frac{R}{K} \cdot \frac{\int_0^H Q_r(z)dz}{\sum_{n=1}^{\infty} \frac{\beta_n^2+\gamma_n^2}{\beta_n\gamma_n} \cdot \sin(\beta_n R)\sin(\gamma_n H)} \\ &\cdot \sum_{n=1}^{\infty} \left[1 - \exp\left(-a\beta_n^2\tau\right) \cdot \exp\left(-a\gamma_n^2\tau\right)\right] \cos(\beta_n r)\cos(\gamma_n z).\end{aligned} \quad (18)$$

III. Results

A. Identifying of the Physical Parameters

The values of ac magnetic field density were tested at perpendicular locations, which are shown in Fig. 6.

The parameters of the composite were tested as

$$\begin{aligned}\rho &= 1.02 \times 10^3\ \mathrm{kg/m^3}, \quad \mathrm{C} = 3.8\ \mathrm{kJ/kg^\circ C}, \\ K &= 1.1\ \mathrm{W/m^\circ C}, \\ \xi_{\mathrm{NP}} &= 3.6\ \mathrm{mg/cm^3}\ \text{or}\ \xi_{\mathrm{Fe}} = 2.52\ \mathrm{mg/cm^3}, \\ \mathrm{R} &= 1.4\ \mathrm{cm}, \quad \mathrm{H} = 3.5\ \mathrm{cm}\end{aligned}$$

In the simulation, the heat convection coefficient surrounding the composite is 20 W/m^2°C.

B. Determination of SAR in Phantom Studies

The experimental values of SAR at 6 positions were calculated from the initial temperature transient in the maghemite

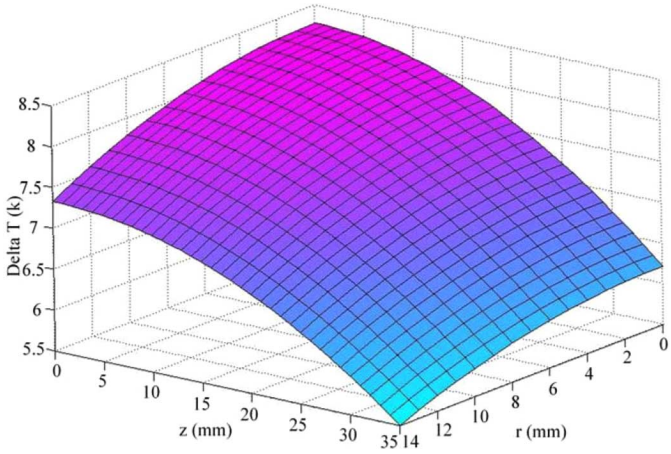

Fig. 7. 3-D graph with simulated results after 2400 s. The temperature ascends to the peak of 8.3 °C and the lowest point of 5.5 °C in the composite model.

-gelled model:

$\mathrm{SAR} = 6.2 \times 10^3$ W/kg of NP or 8.9×10^3 W/kg of Fe, where $\mathrm{z} = 1$ cm, $\mathrm{r} = 0.7$ cm and $\mathrm{r} = 1.4$ cm;

$\mathrm{SAR} = 4.9 \times 10^3$ W/kg of NP or 7.0×10^3 W/kg of Fe, where $\mathrm{z} = 2$ cm, $\mathrm{r} = 0.7$ cm and $\mathrm{r} = 1.4$ cm;

$\mathrm{SAR} = 4.0 \times 10^3$W/kg of NP or 5.7×10^3 W/kg of Fe, where $\mathrm{z} = 3$ cm, $\mathrm{r} = 0.7$ cm and $\mathrm{r} = 1.4$ cm.

C. Comparison of Theoretical and Experimental Values

With respect to the clinical applications, the rise of temperature as a function of time must also be known in order to choose the appropriate heating duration time. Fig. 7 shows the maximum (8.3 °C) of temperature elevating in the model is at the position of $\mathrm{r} = 0$ cm with $\mathrm{z} = 0$ cm, and the minimum (5.5 °C) is at $\mathrm{r} = 1.4$ cm with $\mathrm{z} = 3.5$ cm after 2400 s. The temperature in the model is close to clinical application.

Fig. 8 shows the comparison of simulated results with the experimental data. The curves are from the simulated results and the points are from the data measured by FOTSs, respectively.

Fig. 9 depicts the transient temperature distribution at three specific positions. The quality of initial temperature transient reduces with the vertical distance, corresponding with the attenuation of the field intensity. Due to the heat source generated by the nanoparticles, the highest temperature occurs approximately at the center of the bottom. More than 2400 s is needed for the composite temperature to reach a steady state.

IV. Discussion and Conclusion

The temperature distribution is of great importance in determining how successful the treatment is, that is, how much of the tumor is heated to therapeutic temperatures, and how much of the surrounding normal tissue is damaged by the heat. From (6), we found that the inhomogeneous heating is caused by two factors; the inhomogeneous physical parameters of magnetic field and heterogeneous particles distribution. By the knowledge of these two factors, the thermal model in future will give significantly different results to those for a model of homogeneous heating and thus will be preferable when accurate results are required [11].

In the aperture of the ferrite-core applicator, the attenuation of the intensity of external alternating current magnetic field is focused mainly on the vertical distance, which leads to the SAR values inhomogenous in the maghemite-gelled composite. The values of SAR are detected by FOTSs. Then the heat generations Q_r are acquired in the heat transfer equation. The progressional solution is used to solve the transient heat transfer problem in the cylindrical model. The simulated results are in good agreement with the experimental data.

In this experiment, the magnetic nanoparticles of 77.5 mg were dispersed in the cylindrical model, resulting in the thermal field with appropriate temperature elevation. The temperature ascends to the peak of 8.3 °C and the lowest point of 5.5 °C after 2400 s. The ascending temperature is close to clinical application. Two methods essential in producing the desired temperatures in AEH therapy involve controlling particle dosage in tumor tissue with intravascular administration and regulating physical parameters of external ac magnetic field [19], [20]. The inhomogeneous model can also help control temperature during treatments by simulation. In this paper, we developed the particular SAR measurement for simulation. The SAR value depends on the physical parameters of ac magnetic field. Changing the external magnetic field can regulate the SAR distribution in the model, allowing the temperature distribution to be adjusted according to clinical requirement.

In the BHT equation, the magnetic particles' spatial distribution can be theoretical considered and in the clinical therapy the area of NP distribution can be identified by CT. When the particles are taken as thousands of heat resources in the external ac magnetic field, the SAR values and particle distribution should be taken as function of space.

In the simplified phantom *in vitro*, the agreement between measured temperatures and the values numerically simulated is satisfying. The accurate inhomogeneous model in future could possibly be applied in the hyperthermia treatment planning and help optimize the surgical procedures. In treatment planning of tumor hyperthermia with magnetic nanoparticles, the information obtained from the theoretical prediction could be beneficial for achieving a complete tumor destruction and minimal surrounding tissue damage [8].Therefore, clinical trials to treat HCC by AEH seem to be possible on the base of a procedure which is carefully planned by means of simulation calculations.

However, there is still a lot of work to be done before achieving the accurate simulation *in vivo*, especially with respect to inhomogeneous distribution of the magnetic material in the highly variable texture and vascellum of the tumor. To attain this, the blood perfusion rate, of smaller than normal tissue, should be more accurately determined. In addition, the complex boundary conditions in the phantom and local thermal parameters of the cancerous tissue should be investigated in more detail.

Our further study will concentrate on the simulation of liver tumor model in rabbits. Many factors that affect the accuracy of the simulation will be considered and experiments will be

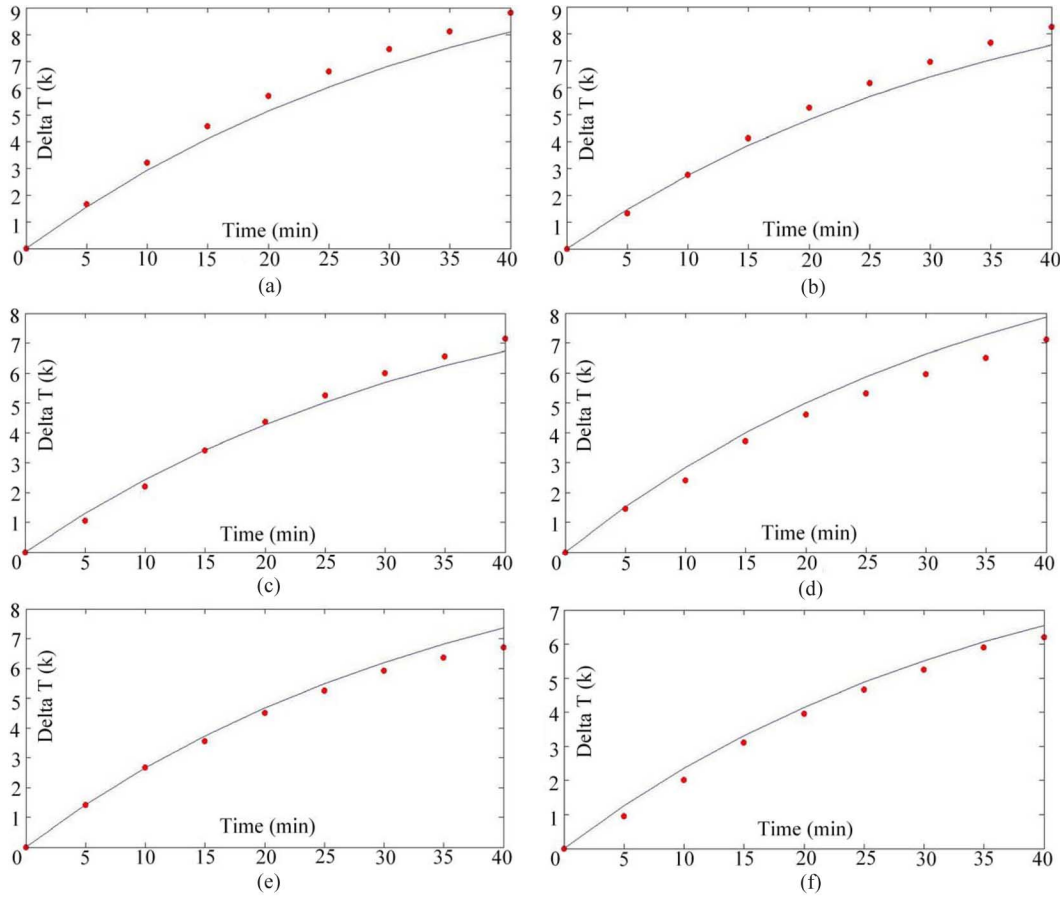

Fig. 8. Comparison of simulated results with the experimental data. (a). $r = 0$ cm with $z = 1$ cm, (b). $r = 0$ cm with $z = 2$ cm, (c). $r = 0$ cm with $z = 3$ cm, (d). $r = 0.7$ cm with $z = 1$ cm, (e). $r = 0.7$ cm with $z = 2$ cm, (f). $r = 0.7$ cm with $z = 3$ cm, where r is the radius and z is the height of the cylindrical composite. The curves are from the simulated results and the points are from the data measured by FOTSs, respectively. The maximum of the relative errors is 9.7%.

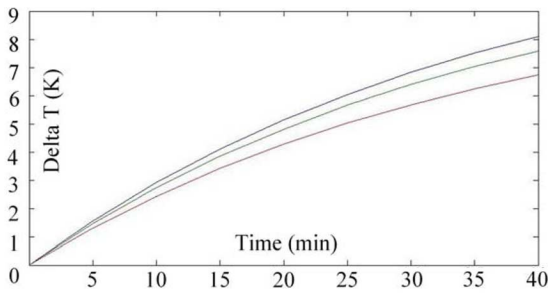

Fig. 9. Time-dependent temperature increase at three specific positions: ($r = 0, z = 1$ cm), ($r = 0, z = 2$ cm), ($r = 0, z = 3$ cm), from top to bottom. The values of SAR were determinable by the initial temperature transient in the maghemite-gelled composite, indicating that the attenuation of magnetic field intensity is mainly focused on the vertical distance of the aperture of the apparatus.

conducted to compare the theoretical results with experimental data. Thus, the computer-aided simulation will deeply impact the clinical therapy for patients in the future.

ACKNOWLEDGMENT

This work was supported by 863 Project of China (No. 6407033158).

REFERENCES

[1] A. Jordan, R. Scholz, P. Wust, H. Fähling, and R. Felix, "Magnetic fluid hyperthermia (MFH): Cancer treatment with AC magnetic field induced excitation of biocompatible superparamagnetic nanoparticles," *J. Magn. Magn. Mater.*, vol. 201, pp. 413–419, 1999.

[2] A. Jordan, R. Scholz, K. Maier-Hauff, M. Johannsen, P. Wust, J. Nadobny, H. Schirra, H. Schmidt, S. Deger, S. Loening, W. Lanksch, and R. Felix, "Presentation of a new magnetic field therapy system for the treatment of human solid tumors with magnetic fluid hyperthermia," *J. Magn. Magn. Mater.*, vol. 225, pp. 118–126, 2001.

[3] N. Siauve, L. Nicolas, C. Vollaire, A. Nicolas, and J. A. Vasconcelos, "Optimization of 3-D SAR distribution in local RF hyperthermia," *IEEE Trans. Magn.*, vol. 40, no. 2, pp. 1264–1267, Mar. 2004.

[4] M. Ma, Y. Wu, J. Zhou, Y. Sun, Y. Zhang, and N. Gu, "Size dependence of specific power absorption of Fe_3O_4 particles in AC magnetic field," *J. Magn. Magn. Mater.*, vol. 268, pp. 33–39, 2004.

[5] M. Johannsen, B. Thiesen, A. Jordan, K. Taymoorian, U. Gneveckow, N. Waldöfner, R. Scholz, M. Koch, M. Lein, K. Jung, and S. A. Loening, "Magnetic fluid hyperthermia (MFH) reduces prostate cancer growth in the orthotopic dunning R3327 rat model," *J. Prostate*, vol. 64, pp. 283–292, 2005.

[6] P. Moroz, S. K. Jones, and B. N. Gray, "Arterial embolization hyperthermia in porcine renal tissue," *J. Surg. Res.*, vol. 105, pp. 209–214, 2002.

[7] P. Moroz, S. K. Jones, J. Winter, and B. N. Gray, "Targeting liver tumors with hyperthermia: Ferromagnetic embolization in a rabbit liver tumor model," *J. Surg. Oncol.*, vol. 78, pp. 22–29, 2001.

[8] Y. Lv, Z. Deng, and J. Liu, "3-D numerical study on the induced heating effects of embedded micro/nanoparticles on human body subject to external medical electromagnetic field," *IEEE Trans. Nanobiosci.*, vol. 4, no. 4, pp. 284–294, Dec. 2005.

[9] P. Liang, B. Dong, X. Yu, D. Yu, Z. Cheng, L. Su, J. Peng, Q. Nan, and H. Wang, "Computer-aided dynamic simulation of microwave-induced thermal distribution in coagulation of liver cancer," *IEEE Trans. Biomed. Eng.*, vol. 48, no. 7, pp. 821–829, Jul. 2001.

[10] W. Andra, C. G. d'Ambiy, R. Hergt, I. Hilger, and W. A. Kaiser, "Temperature distribution as function of time around a small spherical heat source of local magnetic hyperthermia," *J. Magn. Magn. Mater.*, vol. 194, pp. 197–203, 1999.

[11] N. Tsafnat, G. Tsafnat, T. D. Lambert, and S. K. Jones, "Modelling heating of liver tumours with heterogeneous magnetic microsphere deposition," *J. Phys. Med. Biol.*, vol. 50, pp. 2937–2953, 2005.

[12] A. M. Granov, O. V. Muratov, and V. F. Frolov, "Problems in the local hyperthermia of inductively heated embolized tissues," *J. Theor. Found. Chem. Eng.*, vol. 36, pp. 63–66, 2002.

[13] S. Maenosono and S. Saita, "Theoretical assessment of FePt nanoparticles as heating elements for magnetic hyperthermia," *IEEE Trans. Magn.*, vol. 42, no. 6, pp. 1638–1642, Jun. 2006.

[14] H. H. Pennes, "Analysis of tissue and arterial temperature in the resting human forearm," *J. Appl. Physiol.*, vol. 1, pp. 93–122, 1948.

[15] M. M. Chen, K. R. Holmes, and V. Rupinskas, "Pulse-decay method for measuring the thermal conductivity of living tissues," *ASME J. Biomech. Eng.*, vol. 103, pp. 253–260, 1981.

[16] S. Weinbaum, L. M. Jiji, and D. E. Lemona, "Theory and experiment for the effect of vascular microstructure on surface tissue heat transfer—Part I: Anatomical foundation and model conceptualization," *ASME J. Biomech. Eng.*, vol. 106, pp. 321–320, 1986.

[17] Q. A. Pankhurst, J. Connolly, S. K. Jones, and J. Dobson, "Application of magnetic nanoparticles in biomedicine," *J. Phys. D: Appl. Phys.*, vol. 36, pp. 167–181, 2003.

[18] R. E. Rosensweig, "Heating magnetic fluid with alternating magnetic field," *J. Magn. Magn. Mater.*, vol. 252, pp. 370–374, 2002.

[19] S. Bae, S. W. Lee, Y. Takemura, E. Yamashita, J. Kunisaki, S. Zurn, and C. S. Kim, "Dependence of frequency and magnetic field on self-heating characteristics of $NiFe_2O_4$ nanoparticles for hyperthermia," *IEEE Trans. Magn.*, vol. 42, no. 10, pp. 3566–3568, Oct. 2006.

[20] J. Oya, H. Shoji, F. Sato, H. Matsuki, S. Satomi, Y. Nihei, Y. Kurokawa, and T. Sato, "Thermotherapy with metallic stent excited by the magnetic field," *IEEE Trans. Magn.*, vol. 42, no. 10, pp. 3593–3595, Oct. 2006.

Manuscript received June 26, 2006; revised November 22, 2006. Corresponding author: N. Gu (e-mail: guning@seu.edu.cn).